Applied Acoustics 240 (2025) 110933

Contents lists available at ScienceDirect

Applied Acoustics

journal homepage: www.elsevier.com/locate/apacoust

Boundary conditions for hybrid simulations in a rectangular environment with sound-absorbing ceiling

Giulia Fratoni, Dario D'Orazio,*

Department of Industrial Engineering (DIN), University of Bologna, Italy

ARTICLE INFO

Keywords:
Wave-based simulations
Boundary conditions
Non-uniform absorption distribution
Absorption coefficients

ABSTRACT

Acoustic numerical models facilitate sound field prediction in challenging real-world scenarios, such as environments with non-uniform sound absorption distribution. The accuracy of their results strongly depends on the reliability of boundary conditions required as input data. Research has largely covered analytical models of pressure-based boundary conditions for wave-based simulation techniques. However, accessible lists of frequency-dependent acoustic impedances remain limited compared to the energy-based datasets widely available in the literature. Consequently, random-incidence absorption coefficients are often converted into complex surface impedances through non-unique processes. This work explores the potential discrepancies between the input data of a wave-based finite-element model (hybridized with ray-tracing), and the energy-based coefficients employed in analytical predictions and geometrical acoustics simulations. The 3D model of an existing rectangular space with a highly sound-absorbing surface (the ceiling) is a suitable test environment for this investigation. Room criteria obtained with in-field acoustic measurements, i.e., reverberation time and speech clarity, are the experimental reference data throughout the work. Focusing on the air-backed sound-absorbing tiles at the suspended ceiling, results reveal gaps in input data, suggesting a potential percentage of discrepancies between the analytical formula and numerical models' input data up to 25% at low-mid frequencies (125 Hz - 250 Hz - 500 Hz).

1. Introduction

The reliability of boundary conditions is essential for achieving accurate results during the acoustic design process. Nowadays, engineers, architects, acousticians, and researchers benefit from extensive collections and available datasets of random-incidence sound absorption coefficients [1,2]. ISO 354 and ASTM C423 standards are the internationally recognized procedures to characterize products' acoustic performance in reverberation chambers [3,4], notwithstanding reproducibility and uncertainty issues [5–8]. Sabine and Eyring's analytical formulas employ sound absorption coefficients to predict the reverberation time on uniform absorption and diffuse sound field assumptions [9,10]. Further formulas predict reverberation in spaces with non-uniform distribution considering the absorption in the room's three dimensions [11–13]. The geometrical acoustics (GA) modeling techniques help simulate acoustic fields in real-world scenarios with non-diffuse sound fields employing sound absorption and scattering coefficients [14,15]. As part of the GA-based approaches and originally developed in the '60s for large performance spaces [16,17], ray-tracing methods are now widely applied to everyday-life spaces, such as learning and working environments [18,19].

In recent decades, wave-based (WB) models have become a numerical tool increasingly adopted for room acoustic simulations [20–23]. Wave-based simulations were previously used for low-frequency analysis and small rooms due to their inherent high computational costs. Optimized codes and parallel computation through Graphics Processing Units (GPUs) have mitigated such drawbacks, facilitating their use for higher frequencies and larger volumes [24,25]. Wave-based approaches, such as finite-element, boundary-element, and finite-difference methods, necessitate the specification of the surface acoustic impedance to model the interaction of the sound field with the acoustic boundary [26–28]. Despite the growing applications of WB simulations in room acoustics, the availability of pressure-based quantities, such as complex acoustic impedances or reflection factors, still remains an active area of research [29–31]. Consequently, using WB models as acoustic design tools often involves converting the widely available energy-based quantities into acoustic impedances. Even though this conversion process inevitably yields non-unique solutions, scholars proposed and validated

* Corresponding author.
E-mail address: dario.dorazio@unibo.it (D. D'Orazio).

https://doi.org/10.1016/j.apacoust.2025.110933
Received 15 July 2024; Received in revised form 4 June 2025; Accepted 4 July 2025
Available online 9 July 2025

robust methods to convert random incidence sound absorption coefficients to complex surface impedances, using prior information about the absorber model as constraints [32]. The practical implications of such retrieving processes need further investigation, especially when considering commercial products' technical data or composite non-trivial materials. In those cases, the available information on the materials' acoustic performance involves α measured through ISO 354 or ASTM C423. Deriving the required adjustments of sound absorption coefficients depending on the material model involved is crucial for accurate room criteria predictions.

Previous works by the authors explored this aspect in large complex geometries using finite-difference time-domain [33,34] or finite-element methods [35] hybridized with ray-based solvers. In some of these works, the focus was on material properties assigned to critical groups of surfaces, i.e., those constituting the theatre boxes and the upholstered seats' rows in the stalls. The main findings highlighted a variation up to 45% at low frequencies from the energy parameters assigned to the surfaces in GA simulations to those employed to retrieve the acoustic admittances used in WB simulation [36].

The present investigation attempts to quantify to what extent the available α coefficients of sound-absorbing ceilings could need corrections to obtain the boundary conditions for hybrid wave/ray-based simulations. This work focuses on the differences in input data between a hybrid wave/ray-based engine and two conventional prediction tools: the Sabine formula and a state-of-the-art geometrical acoustics model. A mid-sized room with acoustic treatments at the ceiling was chosen for the intended analysis. Its frequency-dependent reverberation time values were analytically predicted through EN 12354-6 formula, simulated with GA and hybrid models, and measured through in-field acoustic campaigns according to ISO 3382-2.

This article is organized as follows. Section 2 gives a brief overview of the background theory on room boundaries. Section 3 describes the analytical formula employed to predict reverberation time, the in-field acoustic measurements, and the numerical models used in the present work. Section 4 presents the main outcomes regarding input data discrepancies among the different methods. Finally, Section 5 outlines the main conclusions of this study, along with its inherent limitations. The current paper is intended to continue and expand the outcomes presented in [36].

2. Room boundaries: theoretical background

In the general case of a boundary hit by a sound wave, R is the ratio of the reflected pressure, p_r, to the incident pressure, p_i:

$$R = \frac{p_r}{p_i} = |R|e^{i\chi} \tag{1}$$

where $|R|$ represents the magnitude and χ denotes the phase of the reflected sound wave. The reflection factor R completely characterizes a surface's acoustic performance in terms of incidence angle and frequency. The complex specific acoustic impedance is the ratio of the sound pressure at the surface, p, to the normal component of the particle velocity, v_n, at the incidence point:

$$Z = \frac{p}{v_n}. \tag{2}$$

The normalized specific acoustic impedance is written as $\zeta = Z/\rho_0 c_0$, where $\rho_0 c_0$ is the characteristic acoustic impedance of the air ($\simeq 415\,\mathrm{kg/m^2 s}$ at 20 °C), and its inverse value is defined as the admittance $\gamma = 1/\zeta$.

For plane waves incident on infinite surfaces, the relation between the absorbed energy and the incident energy is given by

$$\alpha = 1 - |R|^2, \tag{3}$$

where α is the sound absorption coefficient (the fraction of intensity lost during reflection). In case of normal-incident wave ($\theta = 0$):

$$R = \frac{Z_s - \rho_0 c_0}{Z_s + \rho_0 c_0} = \frac{\zeta - 1}{\zeta + 1}, \tag{4}$$

and consequently:

$$\alpha(\zeta) = \frac{4\mathrm{Re}(\zeta)}{|\zeta|^2 + 2\mathrm{Re}(\zeta) + 1}. \tag{5}$$

Handling wave-based numerical models may require the conversion from α to R (or Z, ζ, γ) due to the lack of extensive datasets of complex boundary conditions. Previous studies developed a general impedance model based on a damped oscillator to retrieve theoretical surface impedances using existing data [32,37]. Such an inverse method was created to convert absorption coefficients from reverberation chambers into surface impedances by solving a constrained optimization problem. Further research presented a method for estimating the impedance of common materials at low frequencies, incorporating local reaction assumption and determining the amplitude and phase of the complex pressure reflection factor [38]. Despite the inherent non-uniqueness of the process, researchers agree on combining input absorption coefficients with the prior information on the absorbing behavior of interest.

While converting absorption coefficients to surface impedances, the optimization problem can be generally expressed as:

$$F(\zeta) = |\alpha_{\gamma eq} - \alpha_{input}|^2, \tag{6}$$

where $F(\zeta)$ is the optimization function, $\alpha_{\gamma eq}$ is the absorption coefficient corresponding to ζ, and α_{input} is the absorption coefficient provided as input data. The goal is to minimize the optimization function utilizing the restrictions provided by the absorber's analytical model.

3. Method

3.1. The case study

The environment examined is a secondary school classroom hosting up to 25 students in a volume of 159 m^3. The room has a parallelepiped shape and is furnished with closets, wooden chairs, and desks. The floor is entirely uncarpeted. The main characteristics of the room are outlined in Table 1.

Table 1
Features of the room selected as a test environment for the study.

Room features	
Room's volume	$V = 159\ m^3$
Ceiling surface	$S_{ceiling} = 53\ m^2$
Room's height	$H = 3$ m
Maximum occupancy	$N = 25$
Seating area's furniture	Wooden chairs and desks
Extra furniture	Closets
Carpet (yes/no)	no

As ceiling materials are crucial for controlling room acoustic parameters and intelligibility, the focus is on ceiling absorption properties [39–41]. In the classroom under study, a heterogeneous configuration at the ceiling combines two materials, described hereafter.

- **Material 1**: perforated gypsum board
  Perforation percentage: 18%
  Thickness: 8 mm
  Weight: 7.5 kg/m^2
  Placement: at the center of the ceiling (~ 45% of the total available surface)
  Acoustic performance: significant absorbing properties at 250 Hz, 500 Hz, and 1000 Hz ($\alpha > 0.8$)
- **Material 2**: high-density rock wool
  Density: 70 kg/m^3
  Thickness: 22 mm

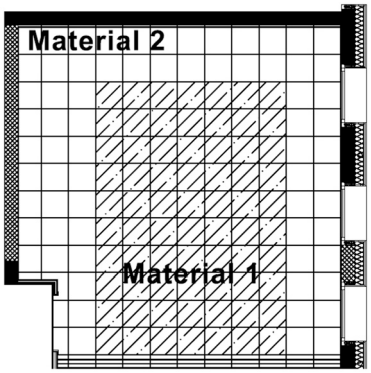

Fig. 1. Ceiling layout: Material 1 at the center (~ 45% of the total available surface) and Material 2 at the perimeter band (~ 55% of the total available surface).

Placement: at the perimeter band of the ceiling (~ 55% of the total available surface)
Acoustic performance: significant absorbing properties from 250 Hz to 4000 Hz ($\alpha > 0.8$)

Fig. 1 shows the layout of the acoustic treatments installed on the ceiling, inspired by standards and existing research [42–45]. The sound absorption coefficients of the ceiling tiles were measured in the reverberation chamber (280 m^3) of the Applied Acoustics Group at the University of Bologna following the procedures outlined in ISO 354. During the first step of ISO 354 measurements (without the specimen), an empty frame with a steel grid arranged for 36 tiles (0.60 m x 0.60 m each) and a 10 cm air gap behind was placed on the reverberation room's floor. Even with such a frame, the laboratory's equivalent absorption area of the empty room (A_1) was in the required ranges in each third-octave band from 100 Hz to 5000 Hz (see Table 1 in Ref. [3]). Then, each specimen was installed on the frame for an overall area equal to 10.8 m^2. The specimen was placed at the center of the reverberant room's floor, avoiding any edges parallel to the walls. The thermo-hygrometric conditions during the measurements were: temperature of 21.6 °C, and relative humidity 48.1%. More details about these measurements are presented in the Ref. [46].

3.2. Analytical predictions

In line with common practice for the ordinary rooms' acoustic design, the Sabine prediction formula has been adopted to calculate the reverberation time T [47]:

$$T = \frac{55.3}{c_0}\frac{V}{A} \quad \text{(s)}, \tag{7}$$

where c_0 is the speed of sound in air (m/s), V is the room's volume (m^3), and A is the total equivalent sound absorption area (m^2). This latter quantity is expressed as:

$$A = \sum_{i=1}^{n} \alpha_i S_i + \sum_{i=j}^{o} A_{obj,j} \quad (m^2), \tag{8}$$

where n is the number of surfaces, α_i is the absorption coefficient of the i-th surface, S_i is the area of the i-th surface (m^2), o is the number of objects, and $A_{obj,j}$ is the equivalent absorption area (m^2) of the j-th object. These input data are generally taken from datasets provided by national and international standards, scientific literature, and product datasets.

Table 2 provides α and A_{obj} values used in the analytical formula for the case under study: the former used for surfaces, such as floor, walls, windows, closets, and ceiling tiles, while the latter for chairs/desks and the occupancy. The predicted T values in octave bands in unoccupied conditions allow for calculating the speech clarity, C_{50}. The analytical

Fig. 2. View of the room selected as a test environment for the study. Dimensional features are provided in Table 1.

C_{50} values were obtained using the *Revised theory* by Barron and Lee [48,49]:

$$C_{50} = 10\log\frac{\frac{100}{r^2} + 31200\frac{T}{V}e^{-0.04r/T}(1 - e^{-0.691/T})}{31200\frac{T}{V}e^{-0.04r/T}e^{-0.691/T}} \quad \text{(dB)}, \tag{9}$$

where r is the source-receiver distance (m), T is the reverberation time (s), and V is the volume of the room (m^3).

3.3. In-field acoustic measurements

The authors conducted acoustic measurements in furnished and unoccupied conditions, in compliance with ISO 3382 [50]. The measurement setup included a custom dodecahedron, a monaural half-inch free-field microphone, and a laptop to manage exponential sine sweep signals (512 k samples at 48 kHz) using the software Dirac (B&K, Version 6). Dirac was also used to export room criteria of interest: the reverberation time T_{20} and the early-to-late ratio C_{50}. The sound source was positioned at the teacher's usual location, while nine receivers were evenly distributed throughout the seating area. The receivers were all placed at the same height, i.e., 1.2 meters above the floor level, as recommended by ISO 3382. The maximum and minimum distance to the sound source (teacher's central position) are 5.6 meters and 1.4 meters, respectively. All the receivers were kept at a minimum distance to walls of 1.2 meters. Fig. 2 shows a view of the classroom during the acoustic measurements.

3.4. 3D models parallel calibration

Two 3D models of the classroom were created using Sketchup software: the first for GA simulations and the second for hybrid wave/ray-based simulations. As depicted in Fig. 3, a general reduction of model complexity has been carried out in both models according to the best practice guidelines [51,52]. Details smaller than 0.2 m were excluded from both models. The layers subdivision within both 3D models includes floor, walls, windows, seats, closets, and acoustic treatments at the ceiling (Material 1 and Material 2).

The main difference between the models is the 3D modeling of each desk-chair pair:

- single boxes (0.4 m x 0.4 m x 0.8 m each) for GA simulations, according to the software manual [53];
- double 2D face for each piece of furnishings for hybrid wave/ray-based simulations, according to the software manual [54].

Moreover, the second model can feature higher levels of detail depending on the chosen transition frequency between the DGFEM and ray-radiosity engines. Therefore, closets were modeled as a single box-shaped object in the first model and as three single boxes (corresponding

Table 2
Sound absorption coefficients, α, and equivalent absorption areas, A_{obj}, used to predict the reverberation time with the analytical formula (see Eq. (8)). Data are provided by literature and standards [1,2,43].

	Surface (m^2)	α					
		125 Hz	250 Hz	500 Hz	1000 Hz	2000 Hz	4000 Hz
Floor (tiles)	53	0.01	0.01	0.02	0.02	0.02	0.02
Walls (gypsumboard)	60	0.10	0.04	0.04	0.04	0.04	0.04
Windows (glass)	11	0.08	0.04	0.03	0.03	0.03	0.03
Closets (wood)	9	0.02	0.02	0.03	0.04	0.04	0.05
Material 1	20[a]	0.31	0.72	0.85	0.72	0.59	0.54
Material 2	25[a]	0.37	0.82	0.84	0.82	0.79	0.71
	n.	A_{obj} (m^2)					
		125 Hz	250 Hz	500 Hz	1000 Hz	2000 Hz	4000 Hz
Chairs (wood)	25	0.02	0.02	0.02	0.04	0.04	0.03
Occupancy	20[b]	0.10	0.15	0.35	0.50	0.50	0.55

[a] Considering 85% of the available ceiling surface.
[b] Considering 80% of the maximum occupancy for active conditions [42,43].

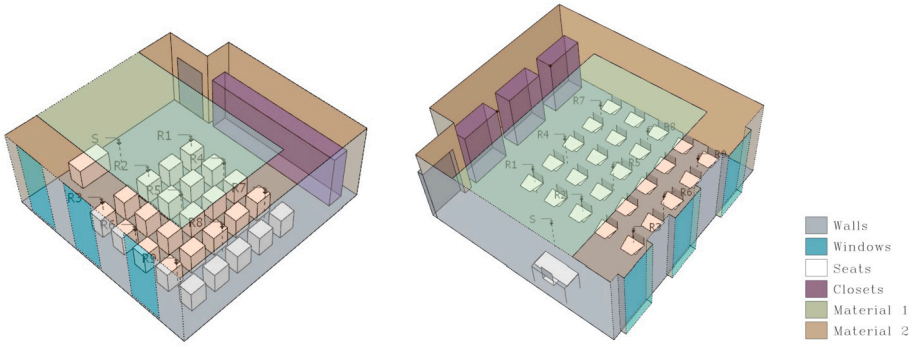

Fig. 3. View of the 3D models employed for GA simulations (left) and hybrid DGFEM/GA simulations (right). Layers subdivision, sound source and receiver locations are also shown (Sketchup software).

to the three actual closets) in the second model. Then, windows and doors were modeled as indentations into the surfaces only within the second model (see Fig. 3). In both 3D models, the virtual sound source and receivers were placed at the same positions as during the measurement campaign.

The first 3D Sketchup model of the room was imported into the GA software Odeon Room Acoustics with the corresponding plug-in [55]. Odeon's algorithm employs the image source method (ISM) up to a certain reflection order and a statistic ray tracing for a higher order of reflections. Given the limited number of surfaces, the transition order (TO) value was set equal to 2 according to the manual's guidelines. For the statistical ray-tracing approach, the authors set 20,000 late rays, while for the whole impulse response, it was a length of 1600 ms. The material properties, i.e., sound absorption (α) and scattering (s) coefficients, were assigned to all the surfaces grouped by material.

The second 3D Sketchup model of the room was imported into a hybrid wave/ray-based simulator with the specific plug-in. This model uses the time-domain discontinuous Galerkin finite-element method (DGFEM) combined with a ray-tracing algorithm for high frequencies analysis [56]. The WB engine of this hybrid room acoustic simulator directly solves the wave equation using the finite element method and iteratively computes the solution by time and space discretizations [24]. The discontinuous Galerkin method is handled with parallel computing clusters and GPUs. At high frequencies, the GA engine combines a pressure-based Image Source Method (ISM) for the initial reflections and a Ray-Radiosity (RR) method for the successive reflections and the scattered energy from the first reflections. The energy histograms generated by the RR method are then processed into an impulse response combined with the ISM output to produce the ray-based impulse response. Then, the DGFEM/GA hybridization process occurs in the frequency domain according to a cross-over frequency chosen by the user. In this case, the transition frequency (TF) was set to 500 Hz to handle the frequency range up to four times the room's Schroeder frequency (around 125 Hz) with the wave-based model. The energy decay threshold was set at 35 dB, allowing for an impulse response length of up to 1.6 seconds. In the ray-based model at higher frequencies, the number of radiosity rays was set to 20,000, and the image source order was set to 2. Besides the dependence on the volume V, the simulation's computational cost depends on the transition frequency elevated to the power of four. With a volume $V = 159$ m^3 and a transition frequency TF = 500 Hz, the time spent on each simulation was around 5 minutes.

The 3D model calibration process generally involves a first assignment of suitable coefficients to the surfaces (grouped by materials) and the iterative plausible adjustment until the match with the measured room criteria, considering a certain tolerance [57]. The tolerance ranges generally refer to the Just Noticeable Differences (JNDs), or their multiples, of each room criterion [58,59].

Table 3 presents the α and s data used in this study at the initial stage of the calibration processes. The parallel calibration of the 3D models was conducted by changing only the ceiling material properties and maintaining the same input data for the rest of the surfaces, such as floors, gypsum board walls, and windows, whose sound absorption coefficients span in a more consolidated range of values in the available datasets [1,2]. This approach enables the evaluation of variations in the boundary conditions applied to the sound-absorbing ceiling tiles. Indeed, while both GA models directly employ α and s data, the energy-based coefficients have been converted into complex reflection factors through the embedded process described in Section 2 for the wave-based part of the hybrid model. In this process, the absorber models assigned to Material 1 and 2 were the "perforated panels" and "porous" embedded

Table 3
Sound absorption coefficients, α, and scattering coefficients, s, used as input data for the GA software (Odeon) and the GA engine of the hybrid DGFEM/GA room acoustics simulator (Treble). The DGFEM solver uses the estimated materials' frequency-dependent complex reflection factors derived from the presented sound absorption coefficients (see Section 2).

	GA simulations input data						
	α						s
	125 Hz	250 Hz	500 Hz	1000 Hz	2000 Hz	4000 Hz	
Floor (tiles)	0.01	0.01	0.02	0.02	0.02	0.02	0.02
Walls (gypsumboard)	0.10	0.04	0.04	0.04	0.04	0.04	0.05
Windows (glass)	0.08	0.04	0.03	0.03	0.03	0.03	0.02
Closets (wood)	0.02	0.02	0.03	0.04	0.04	0.05	0.10
Chairs/desks (wood)	0.04	0.08	0.20	0.22	0.16	0.12	0.30
Material 1 - Initial	*0.26*	*0.61*	*0.72*	*0.61*	*0.50*	*0.46*	0.05
Material 2 - Initial	*0.32*	*0.70*	*0.72*	*0.70*	*0.67*	*0.60*	0.02
	Hybrid DGFEM/GA simulations input data[a]						
	α						s
	125 Hz	250 Hz	500 Hz	1000 Hz	2000 Hz	4000 Hz	
Floor (tiles)	0.01	0.01	0.02	0.02	0.02	0.02	0.10[b]
Walls (gypsumboard)	0.10	0.04	0.04	0.04	0.04	0.04	0.20[b]
Windows (glass)	0.08	0.04	0.03	0.03	0.03	0.03	0.10[b]
Closets (wood)	0.02	0.02	0.03	0.04	0.04	0.05	0.40[b]
Chairs/desks (wood)	0.04	0.08	0.20	0.22	0.16	0.12	0.70[b]
Material 1 - Initial	*0.29*	*0.61*	*0.71*	*0.66*	*0.55*	*0.46*	0.30[b]
Material 2 - Initial	*0.36*	*0.68*	*0.72*	*0.71*	*0.69*	*0.60*	0.30[b]

[a] Frequency-dependent complex reflection factors are derived for the DGFEM engine.
[b] Scattering coefficients in the GA engine (500 - 1000 - 2000 Hz).

models, respectively. Then, the function of Eq. (6) was minimized accordingly. Indeed, the scattering coefficients are assigned to surfaces of GA simulations and the ray-radiosity solver of the hybrid simulator. Both the GA engines accept a single-value s, so that the scattering value is automatically extrapolated to generate a scattering coefficient for each octave band by the algorithms [53,54]. However, Odeon's algorithm combines the user-chosen coefficients and calculations with extra scattering from the size of the surface and distance to the source to obtain the total scattered energy from surfaces. Therefore, the guidelines of the distinct software suggest different s coefficients for various materials. For instance, Treble's guidelines recommend avoiding $s < 0.10$, while Odeon's manual suggests $s = 0.02 - 0.05$ for smooth surfaces. Simulations were run twice for each iteration, according to the state-of-the-art procedure [60,61,57].

The measured frequency-dependent T_{20} values served as the target reference for calibration. The calibration criterion for the 3D model was established by maintaining the discrepancies between measured and simulated T_{20} values within 10% of the measured values [59].

4. Results and discussions

This section outlines the outcomes of the 3D models' calibration, focusing on the average reverberation time across various frequencies. Then, the focus is on the necessary changes in the sound-absorbing characteristics of Material 1 and Material 2 throughout the procedures, specifically from the initial setup (pre-calibration) to the ultimate setup (post-calibration). The calibration has been achieved considering the average $T_{20,occ}$ over the 9 receivers evenly distributed across the seating area (see Fig. 3). The authors considered the occupied state to account for the acoustic conditions in active real-use scenarios. For the same reason, some National Standards define the T requirements in occupied conditions [42,43]. The acoustic contribution of occupancy has been analytically integrated into all datasets, beginning with unoccupied conditions (T_{inocc}), based on the following expression:

$$T_{occ} = \frac{T_{inocc}}{1 + \frac{\Delta A_{pers} T_{inocc}}{0.16V}} \quad (s), \tag{10}$$

where the student's contribution to the equivalent absorption area, ΔA_{pers}, is provided in Table 2 for each octave band [43]. In the present case study 20 students have been considered, corresponding to 80% of the maximum occupancy, as required by DIN 18041 and UNI 11532-2. Table 4 provides:

- the measured average reverberation time in unoccupied conditions, $T_{20,unocc}$, obtained through the acoustic measurements campaign described in Section 3.3,
- the average reverberation time in occupied conditions, $T_{20,occ}$ derived from measurements, analytical formula (see Eq. (7)), and both numerical models (initial and final values) through Eq. (10).

Data provided in Table 4 (occupied state) can be visualized in the first two panels of Fig. 4. The first panel of Fig. 4 depicts the reverberation time across the frequencies before the calibration: the black line represents the measured values, the gray line corresponds to the analytical values, the orange line denotes the calibrated GA model, and the blue line indicates the calibrated hybrid DGFEM/GA model. The initial prediction through the analytical formula returns lower values than the measured one in all the octave bands, as expected. Instead, the main discrepancies between experimental and numerical values are at 125 Hz and 250 Hz. The second panel in Fig. 4 shows the final setup of all the prediction models against the same measured $T_{20,occ}$. Most of the discrepancies between measured and simulated T_{20} values (70%) are below 5% of the measured values, while all the differences are below 10% of the measured values for each octave band [59].

The calibration was validated considering the spatial distribution of speech clarity at 250 Hz ($C_{50,250\,Hz}$). As the early-to-late ratio varies throughout the space, the trend of the speech clarity moving away from the speaker was assessed. The third and the fourth panels of Fig. 4 show the initial and the final set of measured, analytical, and simulated $C_{50,250\,Hz}$ in unoccupied conditions. Values are provided against the source-receiver distance. Considering the mean measured value $C_{50,250\,Hz} = 1.9$ dB, GA and hybrid DGFEM/GA simulations achieved the mean values $C_{50,250\,Hz} = 1.8$ dB and $C_{50,250\,Hz} = 2.7$ dB, respectively. The average has been calculated over the receiver points. Therefore, the

Table 4
Calibration outcomes in terms of $T_{20,unocc}$ and $T_{20,occ}$. The sound source is placed at the teacher's typical position (see Fig. 2), and the 9 receivers distributed across the seating area.

		125 Hz	250 Hz	500 Hz	1000 Hz	2000 Hz	4000 Hz
$T_{20,unocc}$	Measured	1.17	0.81	0.62	0.60	0.68	0.72
$T_{20,occ}$	Measured	1.06	0.74	0.53	0.49	0.54	0.55
	Analytical	1.00	0.61	0.51	0.51	0.55	0.58
	GA (initial)	0.88	0.64	0.54	0.52	0.54	0.54
	GA (final)	1.00	0.66	0.54	0.51	0.54	0.53
	Hybrid DGFEM/GA (initial)	0.86	0.84	0.58	0.54	0.52	0.52
	Hybrid DGFEM/GA (final)	0.98	0.74	0.56	0.54	0.54	0.52

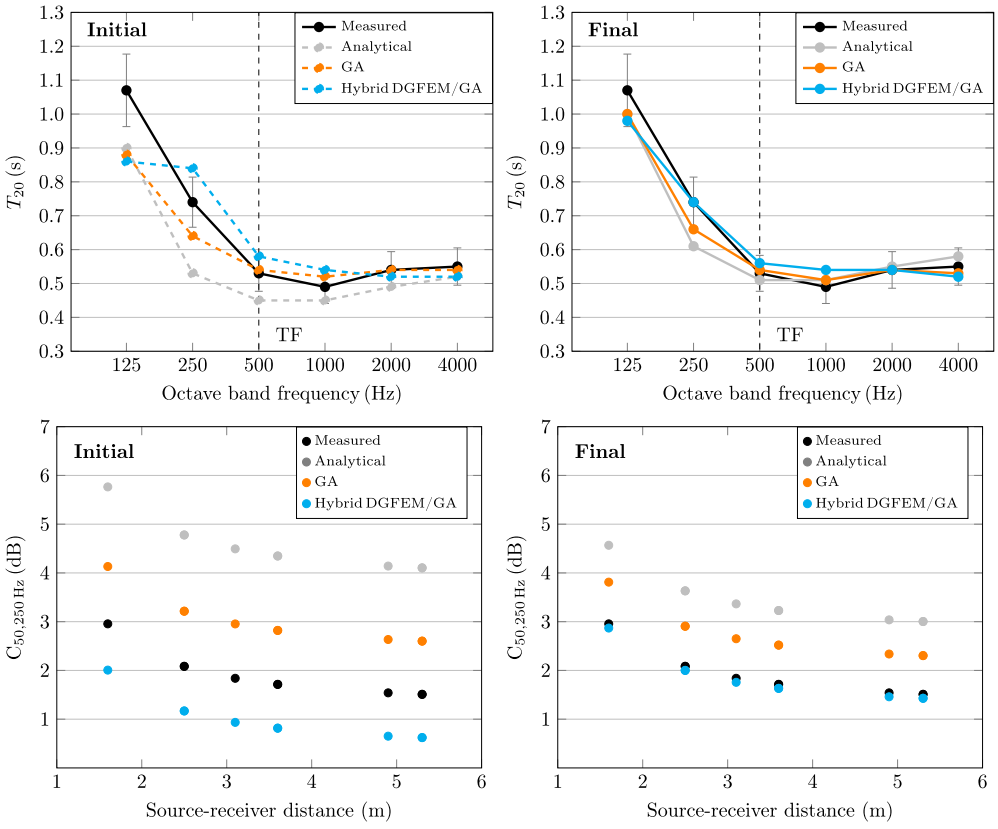

Fig. 4. Measured (black line), analytical (gray lines), GA results (orange line), and hybrid DGFEM/GA results (blue line) at the initial and final step of the calibrations. Reverberation time in occupied conditions $T_{20,occ}$ against the frequency in octave bands (top) and $C_{50,250,Hz}$ in unoccupied state versus the source-receiver distance (bottom). The transition frequency (TF) at 500 Hz is also highlighted.

difference between measured and simulated values is within the sound clarity's JND (1 dB).

Fig. 5 and Table 5 present the α values across octave bands resulting for Material 1 and Material 2 in the final configuration: measured values (black lines), along with the input data of the analytical formula (gray lines), GA simulations (orange lines), and hybrid DGFEM/GA simulations (blue lines). Additionally, the transition frequency between the DGFEM and ray radiosity approaches is indicated (TF = 500 Hz).

In the evaluation of the experimental ISO 354, results from the measurement uncertainties and the usual overestimation of α values were considered [5,7]. The experimental data were adjusted by applying an average γ correction (Fig. 9b in Ref. [6]), considering the range $0.8 < \gamma < 0.9$ with a cautious approach. It is worth noting that these corrections allowed the analytical results shown in Fig. 4 to match experimental T_{20} values. In the absence of any corrections, the predicted T_{20} would have been lower than what was actually obtained (see the gray dashed line in the first panel of Fig. 4).

The resulting gaps between the analytical formula's input data and the coefficients assigned to the numerical model's surfaces, firstly, refer to the effective surface area considered in the distinct approaches. In real-case classrooms, ventilation and lighting fixtures always cover a certain percentage of ceilings, reducing the net available area for acoustic treatments. Depending on the room's dimensions, this percentage is around 15% of the entire ceiling area [46]. When calculating the overall A, the analytical formula directly includes 85% of the S_{floor} surface as the net available area for acoustic treatments, according to the acoustic design best practice. Therefore, net surfaces on the ceiling treated with Material 1 and Material 2 refer to 85% of the corresponding areas, i.e., 45% and 55%, respectively (see Table 2). On the other hand, the 3D digital simplified models typically avoid ventilation and lighting tiles' modeling, as depicted by Fig. 3. Therefore, simulations require a α variation of 15% when assigning material properties to the overall surface to obtain the same total A considered in the analytical formula. The second reason refers to the extra info necessary in numerical models in addition to the α values. While the analytical formula's assumptions include the diffuse sound field conditions ($s = 1$), in ray-based simulations, sound-absorbing properties are combined with the actual scattering coefficients. Previous research outlined higher discrep-

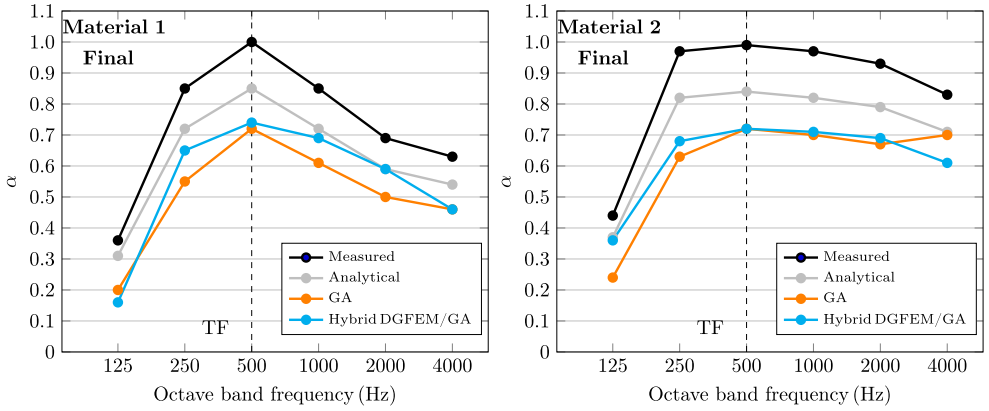

Fig. 5. Sound absorption coefficients in the final configuration. Black lines refer to ISO 354 measurement outcomes; gray lines refer to the input data for the analytical formula; orange lines refer to GA input data, and blue lines refer to the (indirect) input data of the hybrid DGFEM/GA method. The transition frequency (TF) between DGFEM and the ray radiosity approach is at 500 Hz..

Table 5
Measured α (ISO 354), corrected values for analytical formulas (EN 12354-6), GA input data (Odeon), and hybrid DGFEM/GA input data (Treble). In the latter case, the wave-based portion of the engine employs the estimated materials' frequency-dependent complex surface impedance.

		α					
		125 Hz	250 Hz	500 Hz	1000 Hz	2000 Hz	4000 Hz
Material 1	Measured (ISO 354)	0.36	0.85	1.00	0.85	0.69	0.63
	Analytical formula	0.31	0.72	0.85	0.72	0.59	0.54
	GA (final)	0.20	0.55	0.72	0.61	0.50	0.46
	Hybrid DGFEM/GA (final)	0.16	0.65	0.74	0.69	0.59	0.46
Material 2	Measured (ISO 354)	0.44	0.97	0.99	0.97	0.93	0.83
	Analytical formula	0.37	0.82	0.84	0.82	0.79	0.71
	GA (final)	0.24	0.63	0.72	0.70	0.67	0.60
	Hybrid DGFEM/GA (final)	0.36	0.68	0.72	0.71	0.69	0.61

ancies between analytical formulas and GA simulations in classrooms with low scattering values, as the case under study [18].

In the octave bands centered at 125 Hz, 250 Hz, and 500 Hz, the input data of numerical methods (GA and hybrid DGFEM/GA) deviate on average by 25% from those of the analytical formula. For the octave bands centered at 1000 Hz, 2000 Hz, and 4000 Hz, the average deviation remains below 15%. As detailed in Table 5, the percentage error is computed as the ratio between the difference, either "GA (final)" or "Hybrid DGFEM/GA (final)" minus the analytical formula input data, and the analytical formula input data, evaluated for each octave band. Accordingly, the mean error for the low-frequency bands (125 Hz to 500 Hz) ranges between 18% and 25%, based on the average results for Material 1 and Material 2. For the higher-frequency bands (1000 Hz to 4000 Hz), the corresponding error falls within the range of 10% to 15%. Moreover, a comparison of the α values obtained from the GA and hybrid DGFEM/GA methods, as presented in Table 5, reveals percentage differences of up to 18%, with an average discrepancy of 6%. Discrepancies at mid-high frequencies can be attributed to the different ways in which the scattering coefficients in the two GA approaches are handled. The partially random (scattered) direction can lead to slight variations in the resulting room criteria. For this reason, simulations are typically conducted two or three times for each setup.

While comparing ray-based and hybrid wave/ray-based simulations, the first critical issue concerns the approach to the 3D modeling phase. As described in Section 3.4, the pieces of furnishings have been differently modeled according to the best practice guidelines of each numerical approach. The detail required in a hybrid wave/ray-based solver increases with the transition frequency. As a general guideline, the model can handle details down to a quarter of the transition frequency's wavelength. Therefore, the two approaches potentially have different levels of detail, especially for the pieces of furnishings. However, the

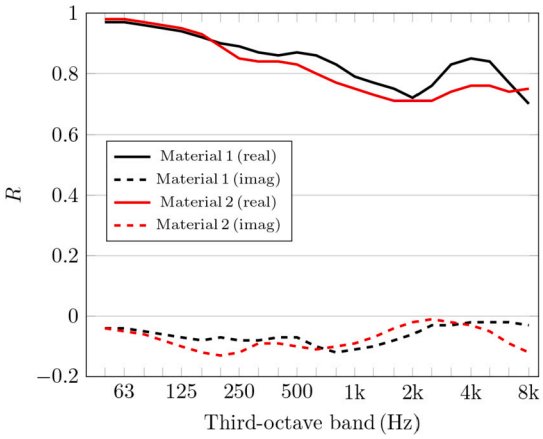

Fig. 6. Normal incidence reflection coefficients' real and imaginary parts assigned to Material 1 and 2 at the room's ceiling in the wave-based engine of the hybrid model [56].

work explores the variation of boundary conditions resulting from two state-of-the-art simulation methods carried out according to the corresponding guidelines.

Moreover, there is an intrinsic uncertainty when comparing coefficients directly assigned in GA simulations with the energy-based coefficients derived from the complex acoustic impedances assigned in WB simulations [32]. The DGFEM simulator adopted in the present study equations (ADE) at the domain's boundaries determines a vector of reflection coefficients that best represent the input absorption coefficients, considering the random incidence angles of the absorption [56]. The algorithm builds a continuous function to represent the reflection coeffi-

cients, as the wave-based solver requires. For instance, Fig. 6 reports the normal incidence reflection coefficients' continuous functions for Material 1 and 2 installed at the room ceiling (real and imaginary parts). The absorption coefficients re-calculated from these continuous functions can slightly deviate from the α original input values. Such deviations are more relevant when there is a high variance between the absorption coefficients in the octave bands.

Finally, the scattering coefficient as input information in GA calculation increases the difficulties and uncertainties while comparing boundary conditions of different simulation approaches. While α values referred to WB models are re-calculated from pressure-based quantities, in GA models they are combined with the effects of scattering coefficients for the room criteria calculations. As a confirmation, when the same absorption and scattering coefficients are used in the ray-based sections of both simulators, the identical input data yield negligible differences in reverberation time values, as observed at 2000 Hz and 4000 Hz.

5. Conclusions

The present paper aims to support scholars and acousticians during the acoustic design of ordinary rooms whose sound absorption distribution is far from being uniform. The uncertainty behind the material properties is a well-known issue in room criteria predictions, and it represents one of the most crucial aspects of room acoustic simulations. Classical analytical formula to predict room criteria relies on sound diffuse field and uniform absorption conditions, that are rare in real-world scenarios. Along with ray-based algorithms, wave-based numerical models offer useful opportunities to predict under more realistic conditions. While GA input data have been largely assessed in literature, the practical implications of converting energy-based to complex boundary conditions need further investigation.

Given the limited availability of pressure-based quantities datasets, this paper outlines potential scenarios on the boundary conditions required by wave-based room acoustics simulators. The current opportunity by hybrid WB/GA commercial room acoustic simulators was exploited to model an existing rectangular room with a common non-uniform sound-absorbing distribution (focused on the ceiling) and a Schroeder frequency of around 125 Hz. The emphasis is given to the boundary conditions assigned to the ceiling surfaces of the 3D model of the room, in comparison with ISO 354 measurements and input data of analytical and GA approaches. The DGFEM model adopted for this work pushed the transition frequency up to 500 Hz before switching to the ray-tracing part of the algorithm. The calibration of the 3D virtual models was achieved based on measured T_{20} for each octave band and checked through the $C_{50,250\,\mathrm{Hz}}$ spatial distribution. The geometries differ in chair modeling in order to provide realistic 3D models adequate for the corresponding simulator. The final input data comparability is granted by using the same virtual geometry as a common starting point and the same room boundaries assigned to all the surfaces (floor, walls, windows, and furnishings) except the ceiling.

The results highlight a potential range of uncertainties for α values while comparing the input data directly used in GA simulations and the α corresponding to the complex acoustic impedances employed in DGFEM part of hybrid simulations. The outcomes suggest considering a potential discrepancy up to 25% at low-mid frequencies and up to 15% at mid-high frequencies.

Although challenging to simulate, the present scenario could also serve as a starting point for comparing room acoustic simulation technologies. The apparent simplicity of the test environment highlights the need for accurate input data to describe surface properties. The same analysis should be addressed in further test environments to expand the outcomes and find more accurate recommendations while handling room boundaries in wave-based simulations. Acousticians and scholars would benefit from the systematic comparison between wave-based models' boundary conditions and random incidence sound absorption coefficients typically employed in analytical formulas and state-of-the-art ray-based simulations.

CRediT authorship contribution statement

Giulia Fratoni: Conceptualization, Writing – original draft, Validation, Investigation, Writing – review & editing, Visualization, Methodology, Data curation. **Dario D'Orazio:** Supervision, Project administration, Resources.

Ethics approval

No human subjects or animals were involved in the research.

Declaration of competing interest

The authors declare that they have no known competing financial interests or personal relationships that could have appeared to influence the work reported in this paper.

Acknowledgements

The authors would like to thank Luca Barbaresi and Domenico De Salvio for their kind support during the acoustic measurements.

Data availability

Data will be made available on request.

References

[1] Vorländer M. Auralization: fundamentals of acoustics, modelling, simulation, algorithms and acoustic virtual reality. Springer; 2020.
[2] Cox T, d'Antonio P. Acoustic absorbers and diffusers: theory, design and application. CRC Press; 2016.
[3] ISO 354:2003 Acoustics—Measurement of sound absorption in a reverberation room.
[4] ASTM C423:2022 Standard Test Method for Sound Absorption and Sound Absorption Coefficients by the Reverberation Room Method.
[5] Wittstock V. Determination of measurement uncertainties in building acoustics by interlaboratory tests. Part 2: sound absorption measured in reverberation rooms. Acta Acust Acust 2018;104(6):999–1008.
[6] Scrosati C, Martellotta F, Pompoli F, Schiavi A, Prato A, D'Orazio D, et al. Towards more reliable measurements of sound absorption coefficient in reverberation rooms: an inter-laboratory test. Appl Acoust 2020;165:107298.
[7] ISO 12999-2:2020 Acoustics — Determination and application of measurement uncertainties in building acoustics.
[8] Jeong C-H, Chang J-H. Reproducibility of the random incidence absorption coefficient converted from the Sabine absorption coefficient. Acta Acust Acust 2015;101(1):99–112.
[9] Sabine WC. Collected papers on acoustics. Harvard University Press; 1922.
[10] Eyring CF. Reverberation time in "dead" rooms. J Acoust Soc Am 1930;1(2A):217–41.
[11] Arau-Puchades H. An improved reverberation formula. Acta Acust Acust 1988;65(4):163–80.
[12] Fitzroy D. Reverberation formula which seems to be more accurate with nonuniform distribution of absorption. J Acoust Soc Am 1959;31(7):893–7.
[13] Zhou X, Späh M, Hengst K, Zhang T. Predicting the reverberation time in rectangular rooms with non-uniform absorption distribution. Appl Acoust 2021;171:107539.
[14] Savioja L, Svensson UP. Overview of geometrical room acoustic modeling techniques. J Acoust Soc Am 2015;138(2):708–30.
[15] Brinkmann F, Aspöck L, Ackermann D, Opdam R, Vorländer M, Weinzierl S. A benchmark for room acoustical simulation. Concept and database. Appl Acoust 2021;176:107867.
[16] Krokstad A, Strom S, Sørsdal S. Calculating the acoustical room response by the use of a ray tracing technique. J Sound Vib 1968;8(1):118–25.
[17] Schroeder MR, Kuttruff K. On frequency response curves in rooms. Comparison of experimental, theoretical, and Monte Carlo results for the average frequency spacing between maxima. J Acoust Soc Am 1962;34(1):76–80.
[18] Bistafa SR, Bradley JS. Predicting reverberation times in a simulated classroom. J Acoust Soc Am 2000;108(4):1721–31.
[19] Keränen J, Saarinen P, Hongisto V. Prediction accuracies of ray-tracing and regression models in open-plan offices. Build Environ 2023;239:110406.
[20] Botteldooren D. Finite-difference time-domain simulation of low-frequency room acoustic problems. J Acoust Soc Am 1995;98(6):3302–8.

[21] Prinn AG. A review of finite element methods for room acoustics. In: Acoustics, vol. 5. MDPI; 2023. p. 367–95.
[22] Wittebol W, Wang H, Hornikx M, Calamia P. A hybrid room acoustic modeling approach combining image source, acoustic diffusion equation, and time-domain discontinuous Galerkin methods. Appl Acoust 2024;223:110068.
[23] Li Y, Meyer J, Lokki T, Cuenca J, Atak O, Desmet W. Benchmarking of finite-difference time-domain method and fast multipole boundary element method for room acoustics. Appl Acoust 2022;191:108662.
[24] Pind F, Engsig-Karup AP, Jeong C-H, Hesthaven JS, Mejling MS, Strømann-Andersen J. Time domain room acoustic simulations using the spectral element method. J Acoust Soc Am 2019;145(6):3299–310.
[25] Bilbao S. Modeling of complex geometries and boundary conditions in finite difference/finite volume time domain room acoustics simulation. IEEE Trans Audio Speech Lang Process 2013;21(7):1524–33.
[26] Kuttruff H. Room acoustics. Crc Press; 2016.
[27] Okuzono T, Yoshida T, Sakagami K. Efficiency of room acoustic simulations with time-domain fem including frequency-dependent absorbing boundary conditions: comparison with frequency-domain fem. Appl Acoust 2021;182:108212.
[28] Aretz M, Vorländer M. Efficient modelling of absorbing boundaries in room acoustic FE simulations. Acta Acust Acust 2010;96(6):1042–50.
[29] Thydal T, Pind F, Jeong C-H, Engsig-Karup AP. Experimental validation and uncertainty quantification in wave-based computational room acoustics. Appl Acoust 2021;178:107939.
[30] Bilbao S, Hamilton B, Botts J, Savioja L. Finite volume time domain room acoustics simulation under general impedance boundary conditions. IEEE/ACM Trans Audio Speech Lang Process 2015;24(1):161–73.
[31] Jeong C-H. Absorption and impedance boundary conditions for phased geometrical-acoustics methods. J Acoust Soc Am 2012;132(4):2347–58.
[32] Mondet B, Brunskog J, Jeong C-H, Rindel JH. From absorption to impedance: enhancing boundary conditions in room acoustic simulations. Appl Acoust 2020;157:106884.
[33] Fratoni G, Hamilton B, D'Orazio D. Rediscovering the acoustics of a XII-century rotunda through FDTD simulation. In: 2021 immersive and 3D audio: from architecture to automotive (I3DA). IEEE; 2021. p. 1–8.
[34] Fratoni G, Hamilton B, D'Orazio D. Feasibility of a finite-difference time-domain model in large-scale acoustic simulations. J Acoust Soc Am 2022;152(1):330–41.
[35] Fratoni G, Tenpierik M, Turrin M, Garai M, D'Orazio D. Acoustic performance of multi-resonator screens in a virtually reconstructed open-plan office. Appl Acoust 2025;229:110381.
[36] Fratoni G, D'Orazio D, Garai M. Uncertainty of input data for wave-based room acoustic simulations in large non-trivial environments. in: Proceedings of Forum Acusticum 2023. Available from: https://doi.org/10.61782/fa.2023.1114.
[37] Mondet BJ-F. Efficient low-frequency room acoustic modelling. Ph.D. Dissertation. Technical. University of Denmark; 2020.
[38] Rindel JH. An impedance model for estimating the complex pressure reflection factor. In: Forum acusticum, vol. 2011. 2011.
[39] Sala E, Viljanen V. Improvement of acoustic conditions for speech communication in classrooms. Appl Acoust 1995;45(1):81–91.
[40] Arvidsson E, Nilsson E, Bard Hagberg D, Karlsson OJ. Quantification of the absorption and scattering effects of diffusers in a room with absorbent ceiling. Buildings 2021;11(12):612.
[41] Nilsson E, Arvidsson E. An energy model for the calculation of room acoustic parameters in rectangular rooms with absorbent ceilings. Appl Sci 2021;11(14):6607.
[42] Deutsche Institut für Normung, Acoustic quality in rooms- specifications and instructions for the room acoustic design. (DIN 18041), Tech. Rep. Deutsche Institut für Normung; 2016.
[43] UNI 11532-2:2020 internal acoustical characteristics of confined spaces — Design methods and evaluation techniques— Part 2: Educational sector (Caratteristiche acustiche interne di ambienti confinati - Metodi di progettazione e tecniche di valutazione - Parte 2: Settore scolastico).
[44] Chandler-Wilde S, Hothersall D. Sound propagation above an inhomogeneous impedance plane. J Sound Vib 1985;98(4):475–91.
[45] Fratoni G, D'Orazio D, Barbaresi L, Garai M, Cappellini L. Mixing materials in false ceilings to increase sound diffusion in education spaces. INTER-NOISE and NOISE-CON congress and conference proceedings, vol. 265. Institute of Noise Control Engineering; 2023. p. 5002–6.
[46] D'Orazio D, Fratoni G, Tardini V. The Italian standard on classroom acoustics UNI 11532-2: 2020 explained through case studies. Appl Acoust 2025;231:110498.
[47] ISO 12354-6:2004 Building acoustics. Estimation of acoustic performance of buildings from the performance of elements Sound absorption in enclosed spaces. UNI 11532-2:2020 Internal acoustical characteristics of confined spaces - Design methods and evaluation techniques.
[48] Marshall LG. Speech intelligibility prediction from calculated C50 values. J Acoust Soc Am 1995;98(5):2845–7.
[49] Barron M, Lee L-J. Energy relations in concert auditoriums. I. J Acoust Soc Am 1988;84(2):618–28.
[50] ISO 3382-2:2008 Acoustics — Measurement of room acoustic parameters. Part 2: Reverberation time in ordinary rooms.
[51] Siltanen S, Lokki T, Savioja L, Lynge Christensen C. Geometry reduction in room acoustics modeling. Acta Acust Acust 2008;94(3):410–8.
[52] Llopis HS, Kjær C, Engsig-Karup AP, Jeong C-H. Just noticeable difference for simulation accuracy between full and reduced order models (l). J Acoust Soc Am 2024;155(1):94–7.
[53] Available from: https://odeon.dk/downloads/user-manual/, March 2025. last view.
[54] Available from: https://docs.treble.tech/user-guide, March 2025, last view.
[55] Naylor GM. Odeon—another hybrid room acoustical model. Appl Acoust 1993;38(2–4):131–43.
[56] Pind F, Jeong C-H, Engsig-Karup AP, Hesthaven JS, Strømann-Andersen J. Time-domain room acoustic simulations with extended-reacting porous absorbers using the discontinuous Galerkin method. J Acoust Soc Am 2020;148(5):2851–63.
[57] Postma BN, Katz BF. Perceptive and objective evaluation of calibrated room acoustic simulation auralizations. J Acoust Soc Am 2016;140(6):4326–37.
[58] ISO 3382-1:2009 Acoustics — Measurement of room acoustic parameters.
[59] Vorländer M. Computer simulations in room acoustics: concepts and uncertainties. J Acoust Soc Am 2013;133(3):1203–13.
[60] Pilch A. Optimization-based method for the calibration of geometrical acoustic models. Appl Acoust 2020;170:107495.
[61] Postma BN, Katz BF. Creation and calibration method of acoustical models for historic virtual reality auralizations. Virtual Real 2015;19:161–80.